Isolates from ancient permafrost help to elucidate species boundaries in *Acanthamoeba castellanii* complex (Amoebozoa: Discosea)

Stas Malavin[*], Lyubov Shmakova

Institute of Physicochemical and Biological Problems in Soil Science RAS, Soil Cryology Lab, Pushchino, Russia
[*] Corresponding author: stas.malavin@gmail.com

Abstract

Acanthamoeba castellanii species complex (genotype T4) comprises of more than ten species with unclear synonymy, as molecular phylogeny has several conflicts with published morphological data. In this paper, we analyze quantitative traits and temperature preferences in six new strains belonging to *A. castellanii* complex isolated from Arctic permafrost in the framework of molecular phylogeny. This integrative approach allows us to cross-link genotypic and phenotypic variability and identify species-level boundaries inside the complex. We also analyze previously known and newly identified discrepancies between the nuclear and mitochondrial gene-based phylogenies. We hypothesize that one reason for these discrepancies may be the intragenomic polymorphism of ribosomal RNA genes.

Key words: Acanthamoeba, genotype T4, permafrost, species concept, species delimitation, rDNA, 18S SSU, intragenomic polymorphism

Introduction

Acanthamoeba is a protist genus belonging to the supergroup Amoebozoa. It has very characteristic angular, or stellate, cysts with an envelope consisting of two distinct layers (Fig 1K, L, M) and fine tapered hyaline projections in the active forms – the so-called acanthopodia (Fig 1A, B, D, E). It is common in soils and aquatic environments all around the world (Geisen *et al.*, 2014). The genus is also known as an opportunistic pathogen causing amoebic keratitis and encephalitis in humans (Khan, 2005; Maycock & Jayaswal, 2016). Due to a well-established method of axenic cultivation, it has become a popular model in biochemical and cell structure studies (Siddiqui & Khan, 2012). *Acanthamoeba* was among the first organisms whose nuclear small subunit ribosomal RNA gene (18S rDNA) sequence was

determined (Gunderson & Sogin, 1986). Its genome is assembled and annotated (Clarke *et al.*, 2013), and several other draft assemblies are present in GenBank.

Despite such a rich history of study (or partially because of it), the system of the genus is surprisingly tangled. The list of described species includes around 30 names. For several of them, the synonymy is apparent from allozyme and molecular data and could also be suspected for some others. Since the beginning of rDNA phylogeny era, several ribotypes (traditionally called “genotypes” in *Acanthamoeba* literature) have been described based on a threshold in genetic distances and characteristic signatures in genus-specific hypervariable regions of the 18S gene. These types were designated T1–T22 (Tice *et al.*, 2016; Corsaro & Venditti, 2018). While some of the types directly correspond to formally described species, others include type strains of several species. This particularly concerns type T4, the most frequently isolated one in both clinics and nature (Maciver *et al.*, 2013). Internally, type T4 is also heterogeneous, which has been noted since the beginning of comparative studies of the 18S rDNA in *Acanthamoeba* (Gast *et al.*, 1996; Fuerst, Booton, & Crary, 2015), though genetic distances between clusters inside T4 are smaller than those between this and the other types (Stothard *et al.*, 1998). Here belong the type strains of most of the species described on the basis of morphology, including the generic type, *Acanthamoeba castellanii* (Douglas, 1930) and thoroughly redescribed by Page (1967) *Acanthamoeba polyphaga* (Puschkarew, 1913). Due to the plastic nature of characters by which T4 species are differentiated and unclear synonymy, some authors prefer to designate this type “*A. castellanii* species complex” (Kong, 2009; Corsaro *et al.*, 2017). Therefore, reconciling molecular with morphological data inside T4 is essential for the system of the genus as a whole, which means establishing a genus-specific species concept integrating phenotypic and genotypic taxonomic markers (Boenigk *et al.*, 2012).

We isolated six new *Acanthamoeba* strains from Arctic permafrost sediments, a specific environment, where they have been buried and trapped in a dormant but viable state. It is shown that in cases when freezing occurs in parallel to sedimentation (which can be proven by geological data), the age of embedded cells corresponds to the age of the permafrost sediments, as both transportation and vital activity is impossible at temperatures below 10°C (Rivkina *et al.*, 2000; Gilichinsky & Rivkina, 2011). Our strains were isolated from the sediments dated from the late Pleistocene to early Holocene. Previously, other eukaryotes, including ciliates (Shatilovich, Stoupin, & Rivkina, 2015), amoebozoans (Shmakova, Bondarenko, & Smirnov, 2016; Shmakova *et al.*, 2018), flagellates (Shatilovich *et al.*, 2009; Stoupin *et al.*, 2012), green algae (Vishnivetskaya, 2009), fungi (Kochkina *et al.*, 2012), and nematodes (Shatilovich *et al.*, 2018) were isolated from the sediments of similar age. Even a higher plant belonging to the genus *Silene* was regenerated from the tissue

of a seed found in the excavated borrowing of a ground squirrel, although the attempts to grow those seeds failed (Yashina *et al.*, 2012).

All isolated *Acanthamoeba* strains belong to ribotype T4. To precisely identify the taxonomic position of the strains, we additionally sequenced nearly full-length 16S (mitochondrial) gene and the barcode region of cytochrome oxidase subunit I (Cox1) gene. Further, we performed morphometrics of all life cycle stages, including cysts formed in different conditions. We also studied the growth of isolated strains at different temperatures. By integrating these data, we identified a species-level boundary within the studied range of variation. Putting morphometrics and ecophysiology of several strains into a broader (almost genus-wide) phylogenetic framework allowed us to figure out which level of genetic heterogeneity corresponds to the species-level difference in phenotypes. Additionally, we analyzed previously known and newly identified discrepancies between the phylogenies based on different genes and hypothesized their origin.

Material and Methods

Sampling and strain isolation

Samples for subsequent enrichment cultivation of amoebae were taken from the intact inner part of the permafrost cores. The cores were obtained in the Gydan Peninsula (Western Siberia), Kolyma Lowland, and Bykovsky Peninsula (Eastern Siberia) by a special drilling technique allowing for the sterility of the sample, as described elsewhere (Gilichinskiy *et al.*, 1989; Shi *et al.*, 1997). The cores were kept frozen during all steps of transportation and laboratory processing, which completely prevents the contamination of the inner material by modern microorganisms (Juck *et al.*, 2005; Gilichinsky & Rivkina, 2011).

Samples of about 1 cm^3 were taken from the cores in a laminar flow hood using a sterile scalpel and put into sterile Petri dishes filled with autoclaved mineral Prescott and James medium (Page, 1988). No bacterial culture was added, as reproducing viable bacteria from permafrost soil formed sufficient food supply for the emerging amoebae. The plates have been checked daily under a phase-contrast inverted microscope, and observed amoebas transferred individually by a tapering Pasteur pipette into new plates, from which clonal cultures were subsequently established.

Culturing and encystment

Strains were maintained as monoclonal bacterized cultures (the bacterial community originated from initial permafrost sample) on 1.5% non-nutrient agar plates with 0,01% cerophyl infusion overlay (Page, 1988) at 18°C. Cultures were passaged

monthly. Cysts formed in such cultures without any special induction one to two weeks after plating.

For axenization, cyst-rich cultures were washed from the agar layer, collected by centrifugation at 1,000×g for 1 min, and treated with 1M HCl for 24 hours. The remaining cysts were then washed thrice with autoclaved distilled water and incubated in sterile proteose-yeast-glucose (PYG) medium (Neff *et al.*, 1964) with 100 U mL^{-1} of penicillin and 0.1 mg mL^{-1} of streptomycin (Sigma-Aldrich). Axenic cultures were maintained in 25 cm^2 culture flasks in the same medium at 18°C and passaged every two weeks.

Three conditions of encystment were tested: “bacterized culture,” “sparse axenic culture,” and “dense axenic culture.” A typical bacterized culture represented the first. Axenic cysts were obtained from cultures grown in 3 mL PYG on 60 mm plates to the monolayer stage. The “sparse axenic culture” conditions were achieved as follows: a subculture of 200 µL was transferred into 3 mL Prescott and James (PJ) mineral medium (Page, 1988) and left for several days. The rest of the cells were scraped and centrifuged at 1,000×g for 1 min, washed with PJ, and left in 3 mL PJ for several days representing the “dense axenic culture” conditions. From now on, we refer to the cysts formed in “bacterized culture” conditions as “bacterized cysts”; to those formed in “sparse axenic culture” conditions as “sparse axenic cysts”; to the cysts formed in “dense axenic culture” conditions as “dense axenic cysts.”

Pseudocysts were obtained from axenic cultures. Cells grown at 18°C in 60 mm Petri dishes (3 mL PYG) up to the monolayer stage were washed once with PJ, collected by centrifugation, and put into 3 mL 5% dimethyl sulfoxide (DMSO) solution in PJ (Kliescikova, Kulda, & Nohynkova, 2011). To test the viability of the obtained pseudocysts, they were put into fresh PYG medium, either immediately or after being completely dry during a week.

Microscopy and measurements

Living trophozoites and cysts were observed and filmed either on slides with petroleum jelly sealing using Leica DM2500 microscope with phase and differential contrast optics or directly in culture using Zeiss Axiostar Plus microscope with phase contrast optics and a water-immersion objective. Nikon DS-Fi3 and Watec WAT-221S digital cameras were used for filming in the first and the second case, correspondingly.

Measurements were performed on a monitor with a calibrated ruler using pictures obtained with a Zeiss Axiostar Plus microscope equipped with a Watec WAT-221S camera. In the case of trophozoites, locomotor forms and rounded cells were measured. The measured parameters in locomotor forms included (1) the longest dimension (“the length”), (2) the dimension perpendicular to the longest and going

through the nucleus (“the width”), (3) the diameter of the nucleus, (4) the diameter of the nucleolus, (5) the maximum width of the hyaloplasm crescent at the anterior edge of the cell. For the rounded cells, cysts, and pseudocysts, the diameter was registered. For the cysts, we also counted the number of ostioles. The counting was done without any special staining using phase contrast optics caused the ostiole complex to appear glowing, which in the case of our strains was found to allow practically unambiguous identification of the ostiole number. The cyst measurements were performed across all three conditions tested (see Culturing and encystment).

Statistical analysis of morphometric characters

All calculations were performed in R v. 3.5.2 (R Core Team, 2019). We assumed no normality assumptions for all variables. For a measure of central tendency, we calculated medians and expressed variation as a median absolute deviation (as implemented in package *stats*; scale factor 1.4826) or a range. Values exceeding three interquartile range around the median were removed as outliers. The statistical significance of median differences was assessed with Kruskal-Wallis rank-sum test (package *stats*) and non-parametric (“permutational”) analysis of variance (PERMANOVA), as implemented in the function *adonis*, package *vegan* v. 2.5-3 (Oksanen *et al.*, 2019). Between-groups pairwise Wilcoxon rank-sum tests with Benjamini & Yekutieli correction for multiple comparisons (package *stats*) was used for the post-hoc comparison. Clustering of the morphometric data was done using the neighbor-joining algorithm on euclidean distances, as implemented in *dist* and *hclust* functions.

Sequence acquisition

DNA was extracted from axenic cultures grown in 60-mm Petri dishes to the stationary phase. Cells were scraped from the plastic and collected by centrifugation as described above. The pellets were washed thrice with autoclaved distilled water and finally resuspended in 100 µL of it. This suspension was subjected to the DNA isolation by ExtractDNA Blood kit (Proteinase K plus SDS based lysis and silica-membrane purification; Evrogen, Russia), according to the manufacturer protocol.

The nuclear SSU rRNA gene (18S), mitochondrial SSU rRNA gene (16S), and the mitochondrially encoded cytochrome c oxidase subunit I gene (Cox1) were amplified, purified by agarose gel electrophoresis, and sequenced on an automated Sanger sequencer in Evrogen Co. (Russia). Details of PCR and sequencing may be found in the Supplementary Material.

GenBank accession numbers for the newly obtained sequences are as follows. 16S: MK100243–MK100248. Cox1: MK105577–MK105582. 18S: MK124583–MK124588.

Phylogenetic analysis

For phylogenetic inference, all available good-quality (nearly) full-length sequences were downloaded from GenBank. MAFFT v. 7.307 L-INS-i algorithm (Katoh & Standley, 2013) was used to align sequences. For 18S, hypervariable regions of the alignment were allocated into a separate partition, where gaps were coded as the fifth state (Simmons & Ochoterena, 2000). A phylogeny was reconstructed by Bayesian analysis of posterior probabilities (Bayesian inference, BI) in MrBayes v.3.2.6 (Ronquist *et al.*, 2012) and maximum likelihood (ML) approach in IQTree v.1.6.6 (Nguyen *et al.*, 2015). The detailed description of phylogenetic methods may be found in Supplementary Material.

Growth at different temperatures

We tested the growth of the isolated strains at 4°C, 11°C, 18°C, 25°C, 32°C, 37°C, 40°C, and 42°C (Δ = 1°C for all). At 4–32°C, only axenic cultures were tested, while to 37–42°C, both axenic and bacterized cultures were exposed. Preliminarily, all temperatures were checked with 40-mm plates (1 mL PYG) in several replicates, to test if growth is possible at all. Axenic cultures for the tests were obtained by transferring 50 µL of a 5-day culture. In the case of bacterized cultures, test plates were inoculated with 50 µL of a two-week culture. This assay was carried out for one week; the cultures were checked daily.

For the temperatures, at which the strains have demonstrated growth or at least persisted successfully, the growth rate was estimated quantitatively. 12-well culture plates, 2 mL of PYG per well, were inoculated with a growing axenic culture as described above. Each strain was tested in two to three replicates per temperature level. The assays were conducted until detached rounded cells started to prevail in the culture. Cells were counted in a hemocytometer each 24 h (each 12 h at 32°C). At 4°C, the experiment lasted for a month, and samples for counting were taken weekly, as observations showed no discernible increase of the cell number. The culture growth was approximated by a logistic curve $N = \frac{L}{1+e^{-k(x-x_0)}}$, where L is the asymptote and k – the logistic growth rate. The approximation was done by Levenberg-Marquardt nonlinear least-squares algorithm as implemented in MINIPACK library interfaced through *minpack.lm* package v.1.2-1 (Elzhov *et al.*, 2016) for R v.3.5.2.

Results

Isolated strains

In total, we have obtained ten *Acanthamoeba* isolates from around 400 studied permafrost sediment samples from East and West Siberia. We have succeeded in cloning and axenization of six out of ten isolates. The location of the sampling sites is shown in Supplementary Fig 2. For the essential characteristics of the cores, see Tab 1.

Table 1 Characteristics of the cores.

Strain	Sampling site	Sediment age	Sediment type	Reference
SCL-am8	Sakha (Yakutia) Republic, Kolyma River bank, Duvanny Yar, retrogressive thaw slump. N 68.628232, E 159.194842	Late Pleistocene	Paleosol (buried cryosol)	Zanina et al., 2011
SCL-am9	Sakha (Yakutia) Republic, Bykovsky Pen. N 71.775537, E 129.330297	Late Pleistocene	Yedoma (“Ice Complex”) deposits. Ice-rich sandy loam with peat inclusions	Schirrmeister et al., 2011
SCL-14-2	Yamalo-Nenets Autonomous District, Gydan Pen. N 71.463875 E 76.992927	Holocene	Flood-plain deposits. Sand and sandy loam with detritus admixture	Demidov *et al.*, 2016
SCL-14-3	Yamalo-Nenets Autonomous District, Gydan Pen. N 71.571362 E 73.499595	Late Pleistocene	Yedoma (“Ice Complex”) deposits. Sandy and clay loams.	Demidov *et al.*, 2016
SCL-14-9	Yamalo-Nenets Autonomous District, Gydan Pen. N 71.463875 E 76.992927	Holocene	Flood-plain deposits. Sand and sandy loam with detritus admixture	Demidov *et al.*, 2016

SCL-14-12	Sakha (Yakutia) Republic, Kolyma Lowland, Anyuy River, Stanchikovsky Yar, retrogressive thaw slump. N 68.365311, E 161.523542	Late Pleistocene	Paleosol (buried cryosol)	Legendre et al., 2014

Microscopy observations

All obtained strains feature typical morphological characters of the genus, i.e., acanthopodia in trophozoites and angular shape of the endocyst, and belong to the morphotype II following Pussard and Pons (1977).

Trophozoites

Trophozoites of all strains readily develop locomotor forms when transferred to fresh medium or the slide. The locomotor form is flattened, with a distinct frontal hyaline area usually occupying about one-fourth of the cell length (Fig 1A–E). Typically, it is elongated in the direction of movement, with a width-to-length ratio of about 0.6 (Fig 1A, B). Occasionally, we have observed locomotor forms with the width equal to or even greater than length (Fig 1C, D). Such forms have been encountered more often in strains SCL-14-2, SCL-14-3, SCL-14-12, and are generally more typical for larger cells. Acanthopodia are absent on the leading lobopodium in locomotor forms, though the hyaline crescent edge has rarely been even for a long time, regularly demonstrating undulations and protrusions. In cells moving irregularly, acanthopodia are present on lobopodia also. At the beginning of an active movement or while changing its way, trophozoites demonstrate sudden extensions of the lobopodium in a new direction similar to the eruptive movements of heterolobose amoebae.

Generally, one vesicular nucleus with a single nucleolus is situated in the central part of the cell in locomotor forms. At temperatures 25 to 32 °C, we have observed multinucleate trophozoites (Fig 1G). Those have always been bigger than the median, while nucleoli have been smaller than in normal cells (Fig 1G).

A single contractile vacuole is usually situated in the rear part of the moving cell (Fig 1A, B). In axenic cultures, the cytoplasm is strongly vacuolated, while in bacterized cultures, the number of vacuoles is found to be considerably lower. A bulbous uroid often appeared in locomotor forms (Fig 1A, C, D), sometimes with adhesive filaments (Fig 1D). Sporadically, we observed a sizeable goblet-like food cup at the rear end of the moving cell (Fig 1E), identically to what was described and figured by Page (1967). This formation was considerably more often found in strain SCL-14-12.

Floating forms have been rarely observed in bacterized cultures. The floating form represents a central body mass with 15–20 radiating pseudopodia up to 15 μm long (Fig 1F).

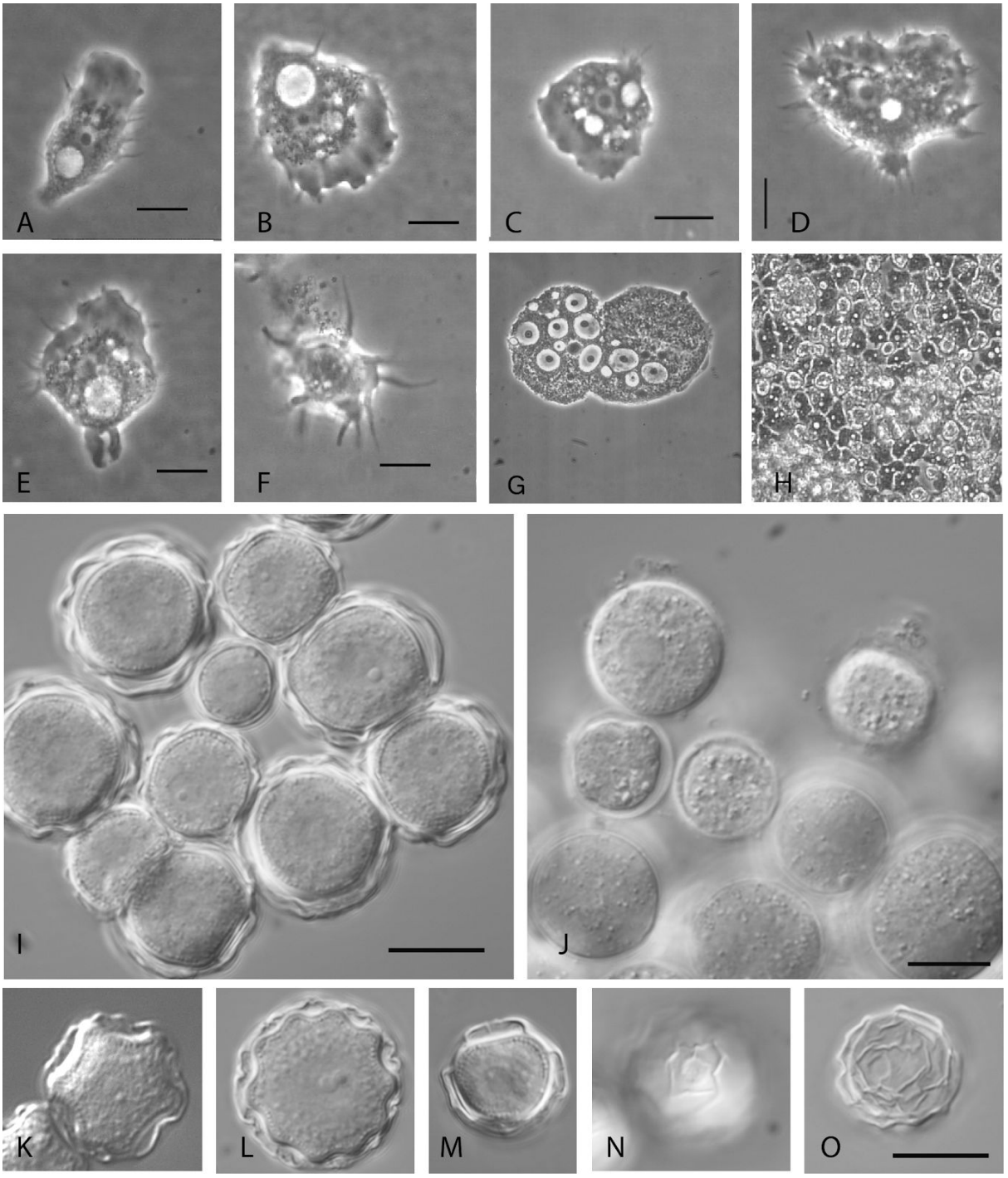

Figure 1 A–E Locomotor forms: A – SCL-14-3; B – SCL-14-3; C – SCL-14-12, D – SCL-am9; E – SCL-14-3; **F** Floating form, SCL-am8; **G** – multinucleate trophozoite, SCL-am9; **H** Monolayer, SCL-14-12; **I, K–N** Cysts, various strains; **J** Pseudocysts, SCL-am8; **O** Empty cyst, SCL-am8.

In axenic cultures grown in plates or culture flasks without agitation, amoebae form a characteristic monolayer on the surface of the substrate (Fig 1H). The “closeness” of the monolayer depends on the temperature and adhesive properties of the plastic

and differs across the vessel area (Fig 1H demonstrates the “ideal” case). After the monolayer reaches its closeness limit, cells start to appear above it massively. This scenario is followed by all studied strains but SCL-14-12, in which cells begin to form compact clumps above the surface from the early stages of the culture growth, in parallel to the monolayer formation.

When the culture is roughly shaken or centrifuged, trophozoites appear as rounded cells without lobopodia and acanthopodia. Such cells demonstrate the internal movement of organelles, though no cell movements can be observed for some time. Similar rounded cells also start to appear soon after an axenic culture reaches its growth limit. In this case, most of them probably die in some time, as the final number of cysts in such cultures is much lower than the number of rounded cells observed at the end of growth.

Cysts

All isolated strains readily encyst in laboratory cultures. In bacterized cultures, all or at least most of the amoebae form cysts in about two weeks after transfer. In axenic cultures, we obtained cysts by transferring amoebae into either the Neff’s encystment medium (Neff *et al.*, 1964) or merely starving PJ medium. When starting to encyst, cells form plaques.

Mature cysts of all strains have well-defined endo- and ectocyst, the former folded and rippled, the latter smoothly polyhedral. Beneath the endocyst, the characteristic layer of oriented granules is always apparent (Fig 1I, K, L, M). The number of endocyst corners usually vary from 3 to 7 (Fig 1I, K, M, O), but cysts with 8 and more corners have also been encountered (Fig 1L). The majority of ostioles lay in one plane. Opperculi do not protrude above the ectocyst level. Dense axenic cysts usually have less prominent endocyst corners than sparse axenic cysts and bacterized culture cysts. In the latter two, a considerable share of cysts has smooth endocyst without any defined corners (Fig 1I).

Pseudocysts

The pseudocyst formation is total only at DMSO concentrations not lower than 5% and when the DMSO-to-cells ratio is not less than the PYG-to-cells ratio during culture growth. In such conditions, all cells transform into pseudocysts in 12 hours. Both dried and non-dried pseudocysts demonstrate almost total viability being put into PYG; in both cases, trophozoites appear in no more than a day.

Pseudocysts are rounded cells with a fine smooth envelope well seen under both phase- and DIC-contrast (Fig 1J). The nucleus is situated in the central area of the cell; the nucleolus is slightly smaller than in trophozoites. The cytoplasm is evenly filled with refractile granules. The size of the granules in pseudocysts is bigger than

that in cysts. No granular layer beneath the envelope characteristic for cysts may be observed.

Molecular phylogeny

18S

The inspection of the preliminary automatic alignment of the T4 18S sequences has revealed six hypervariable regions corresponding to the parts of the third, fifth, sixth, ninth, and eleventh hypervariable ("expansion") regions identified by Gast et al. (1996). Two of those six regions are parts of the diagnostic fragment 3 (DF3) (Booton *et al.*, 2002). The DF3 region is used to distinguish sequence types (Booton *et al.*, 2002; Booton, Kelly, & Fuerst, 2005; Booton *et al.*, 2009), but we have found it sufficient to discriminate between T4 subtypes also, except for some rare cases of closely related sequences. The alignment of concatenated hypervariable regions has yielded easily discernible patterns (Supplementary Fig 4) and has, first of all, demonstrated many several-nucleotide-long indels present in many sequences which by any chance could not be attributed to the alignment method.

Both BI and ML analyses produce seven subtypes, $T4_A$ through $T4_E$ and $T4_{Neff}$, previously mentioned by Fuerst (2014) and Fuerst et al. (2015), further referred to as A–E and Neff. All but A and B receive maximum support in both analyses; B is highly supported (0.9) and A moderately supported (0.78) in the BI analysis. At the same time, the ML and BI trees display one difference in their topologies (Fig. 2). While in both trees the major division lay between the clades A+B and C+F+E, in the ML tree, subtype D appear sister to the A+B clade and subtype Neff sister to subtype E. In the BI tree, vice versa, subtype D is sister to subtype E and subtype Neff sister to the A+B clade.

Several subclusters have got high support in both ML and BI analyses inside clades A and B (Fig. 2). From now on, we refer to them using well-known and long-studied strains they include, for which 16S sequences are also available. This is done for the sake of descriptiveness and does not imply that these strains are somehow "characteristic" of the clusters being described. In clade A, those are "Castellani," "Galka," "Haas," "Rawdon," "Garcia" clades, and one other, not discussed further. In clade B, those are "Ma," "Diamond," "V017" clades, and one other.

In $T4_A$, the topology of the Bayesian tree differs from that of the ML tree (Fig. 3) chiefly by the position of "Haas" clade, which is sister to the cluster containing "Galka" and "Castellani" clades instead of being the deepest $T4_A$ branch as in the ML tree, and the position of "Garcia" clade placed inside "Rawdon" clade instead of being the second deepest branch as in the ML tree.

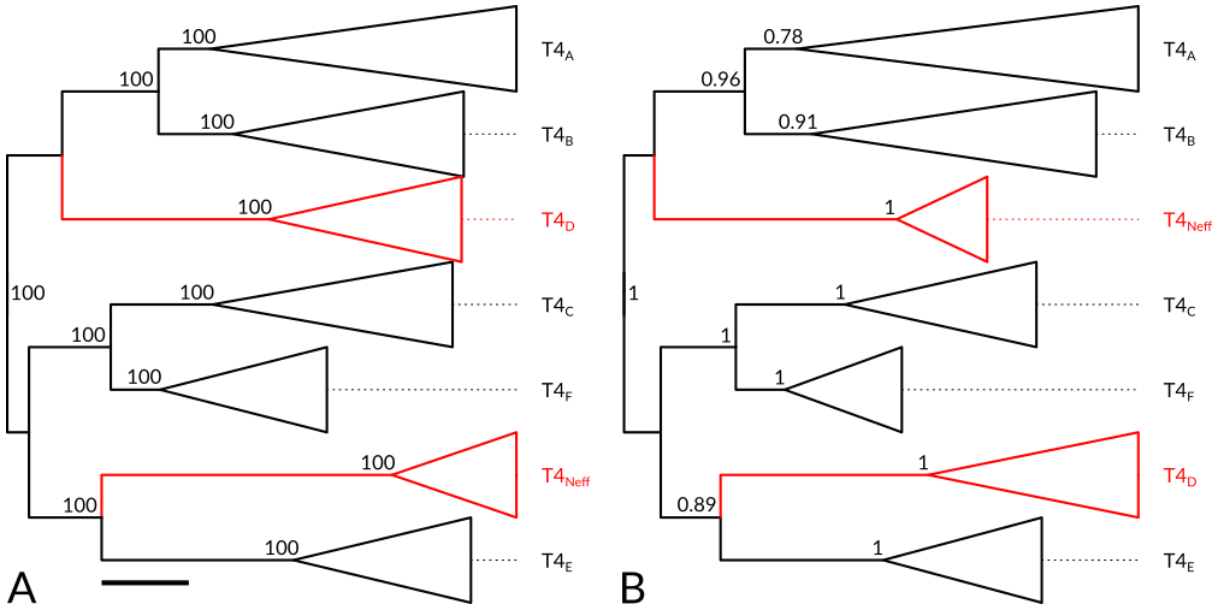

Figure 2 ML (**A**) and BI (**B**) 18S SSU trees of *Acanthamoeba* T4 genotype showing seven subtypes. Branch supports are given as bootstrap percentage / bayesian posterior probability. The trees are rooted at midpoint. Clades with variable position are shown in red. **Scale bar**: 0.01 substitution per site for both A and B.

Strains SCL-am8, SCL-14-2, and SCL-14-3 branch together in the ML tree (Fig. 3) and group with strain COHH 43 from marine sediments of Mt Hope Bay, MA, USA (Gast *et al.*, 2011) as a distinct clade sister to “Ma” clade of $T4_B$. In the BI tree, the permafrost strains and COHH 43 branch before “Ma” clade. Other differences between the BI and ML tree topologies in $T4_B$ involved terminal branching only. Three other permafrost strains grouped within $T4_A$ clade. Strain SCL-14-9 is relatively distant from the other strains except for one clinical isolate KA/E6 from Korea (Liu *et al.*, 2006); their position in the tree is unstable. Strain SCL-am9 is firmly placed into “Galka” clade, and strain SCL-14-12 – into “Castellani” clade.

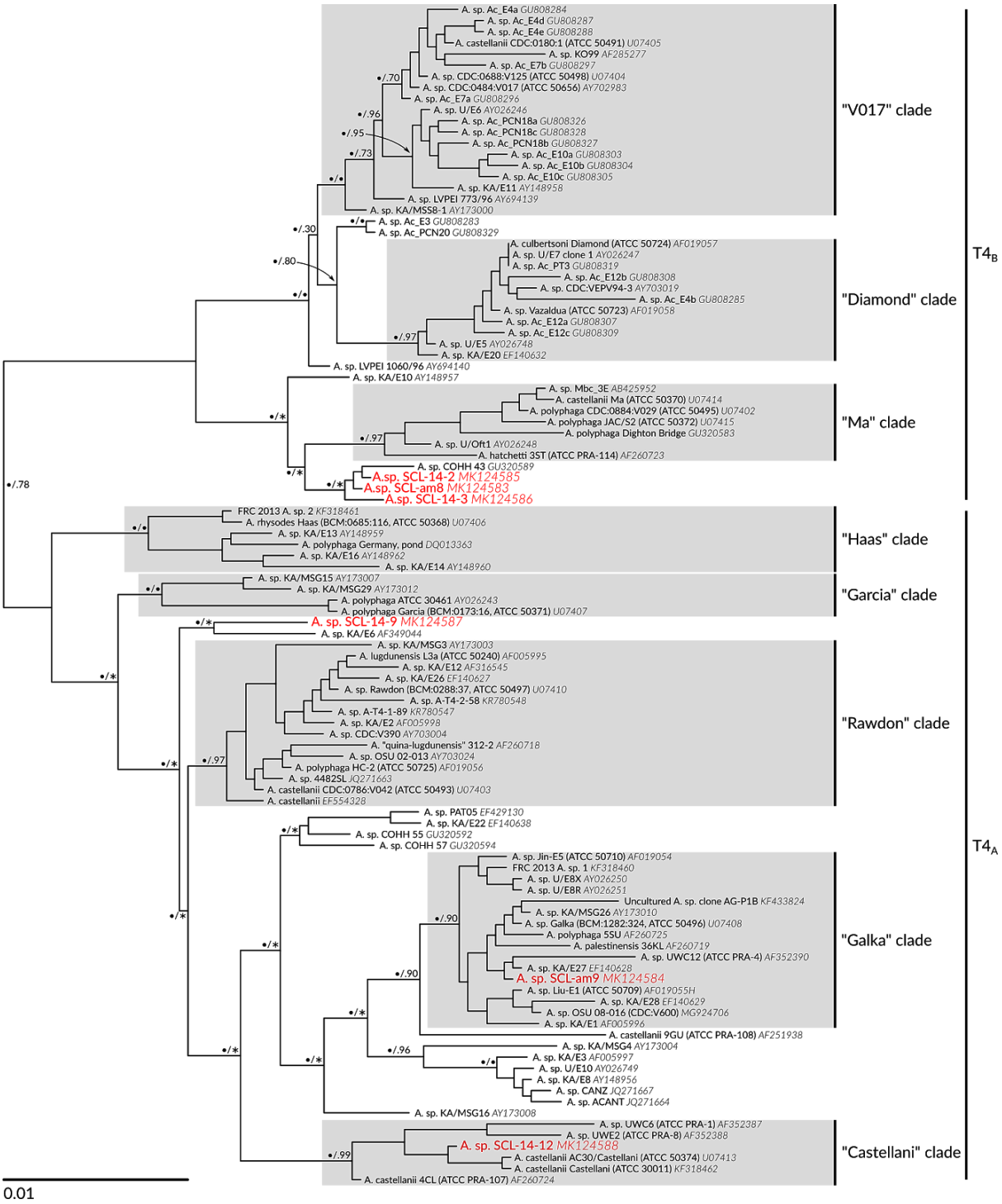

Figure 3 18S SSU ML tree of T4A and T4B clades (a subtree of Fig. 5A, expanded). Bayesian tree gave similar topology (see text). Branch supports are given as bootstrap percentage / posterior probability. • – 100% or 1.00 support; ∗ – clade not observed. Support values inside the clades are omitted. The tree is rooted at midpoint.

16S

The analysis of the 16S alignment confidently recovers all the previously established 18S types for which 16S sequences are available (Fig 4). We thus refer to them further without mentioning in the framework of which analysis are they inferred. Type T4 is moderately supported (94%) in ML-analysis but obtains posterior probability of

1 in BI. T2/6 type is sister to T4 type; the next-closest is T5 followed by T3/T11 clade, though this topology as a whole appears moderately supported. Types T7–T9 (morphogroup I by Pussard and Pons (1977) form a very distinct clade with full support.

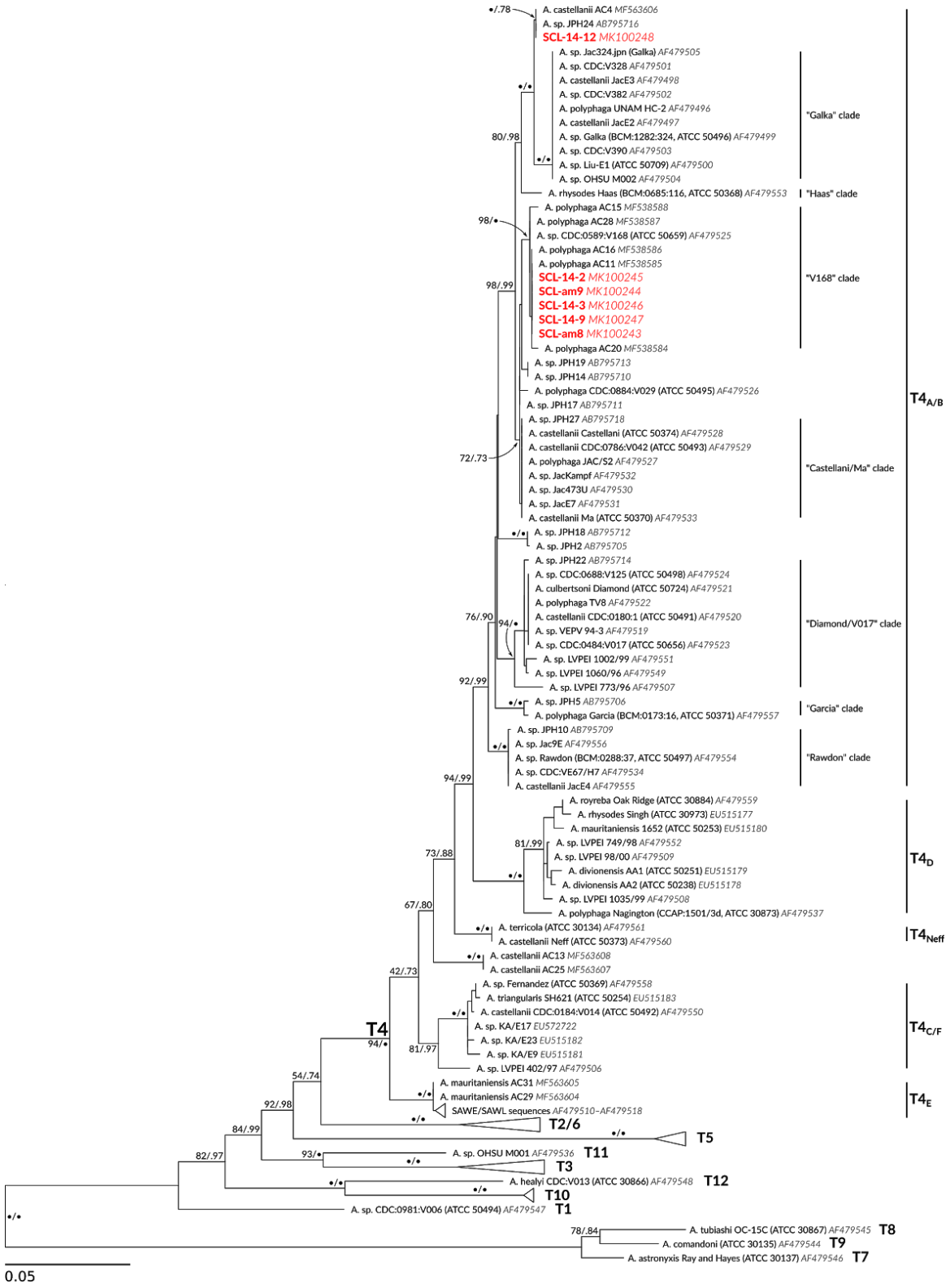

Figure 4 16S SSU ML tree of *Acanthamoeba* T4 genotype. BA tree gave the same topology. Branch supports are given as ML bootstrap percentage / bayesian posterior probability. • – 100% or 1.00 support. Support values near tree tips are omitted. The tree is rooted at midpoint.

The internal structure of 16S-T4 clade partially reflects that of 18S-T4. D, E, and Neff subtypes appear monophyletic with full support. At the same time, subtypes A and B, as well as C and F, are not separate. Subtype E is the most distant from A/B clade, followed by C/F clade, then subtype Neff. Subtype D is the closest to A/B clade. The 16S tree thus corroborates the 18S one inferred with the ML approach, besides the A/B and C/F fusion.

The blended 16S A/B clade, like its 18S separate counterparts, is internally structured (Fig. 4). Galka, Rawdon, and Garcia strains from 18S-T4$_A$ also hit highly supported clusters. Strain Haas does not fall into any cluster but is itself steadily separated. At the same time, strains Castellani and Ma have very similar 16S sequences and form a supported cluster, together with some other strains. The same concerns strains Diamond and CDC:V017.

Surprisingly, all strains from permafrost except SCL-14-12 have identical 16S sequences, also identical to those of strains AC11 and AC16 from India (Megha *et al.*, 2018). In addition to AC15, AC20, AC28, and CDC:V168 (18S-T4$_A$), they form a highly-supported cluster inside T4. SCL-14-12 groups together with Indian AC4 (Megha *et al.*, 2018) and JPH24 from Japan (Rahman *et al.*, 2013) (18S-T4$_B$) as a sister clade to a group containing strains Galka, HC-2, CDC:V390, Liu-E1 (all 18S-T4$_A$), with absolute support. Indian strains AC13 and AC25 reveal rather divergent sequences, probably corresponding to a not yet recovered T4 subtype. Unfortunately, their 18S sequences in GenBank are not full, so it is not possible to either confirm or deny this hypothesis by now.

Cox1

As with the 16S gene, strains belonging to Rns D, E, and Neff subtypes fall into different highly supported clusters, while those within Rns A and B, as well as C and F, form fused clusters (Fig. 5). Clade D groups together with clades C/F, E, and Neff. This subdivision is not supported by ML analysis, though gained 0.97 posterior probability. Inside the C/F/Neff half of the tree, no subtype relationships are confidently resolved.

As with 16S, all permafrost strains, except SCL-14-12, possess identical sequences. Together, they form a supported clade with three sequences from the Ohio State University collection (OSU) 07-033, 07-003 (unfortunately, lacking available 18S sequences) and 07-027 (18S-T4$_A$). A sequence of unknown strain identified as *Acanthamoeba quina* Pussard et Pons, 1977 (genome CDFN) appears sister to that clade with high support. Another highly supported cluster, forming a sister to the just described clade, contains the sequence of strain V017 (Rns T4$_B$), sequences from

genomes CDFL, CDFK, and CDFJ (probably misidentified as *Acanthamoeba pearcei* Nerad, Sawyer, Lewis et McLaughlin, 1993), and a set of OSU sequences belonging to A and B 18S subtypes. Permafrost strain SCL-14-12 groups together with strains OSU 06-024 and 08-016 (both 18S-$T4_A$). One more firm cluster includes the sequence from genome CDFB, identified as *Acanthamoeba lugdunensis* Pussard et Pons, 1977. Other strains in this cluster are Linc Ap-1 (genome LQHA) and two OSU strains, both attributed to 18S-$T4_A$. The last cluster in $T4_{A/B}$ is that encompassing sequences of strain LVPEI 1060/96 (18S-$T4_B$) together with OSU sequences 02-031 (18S-$T4_A$), 05-023 and 07-019 (18S-$T4_B$).

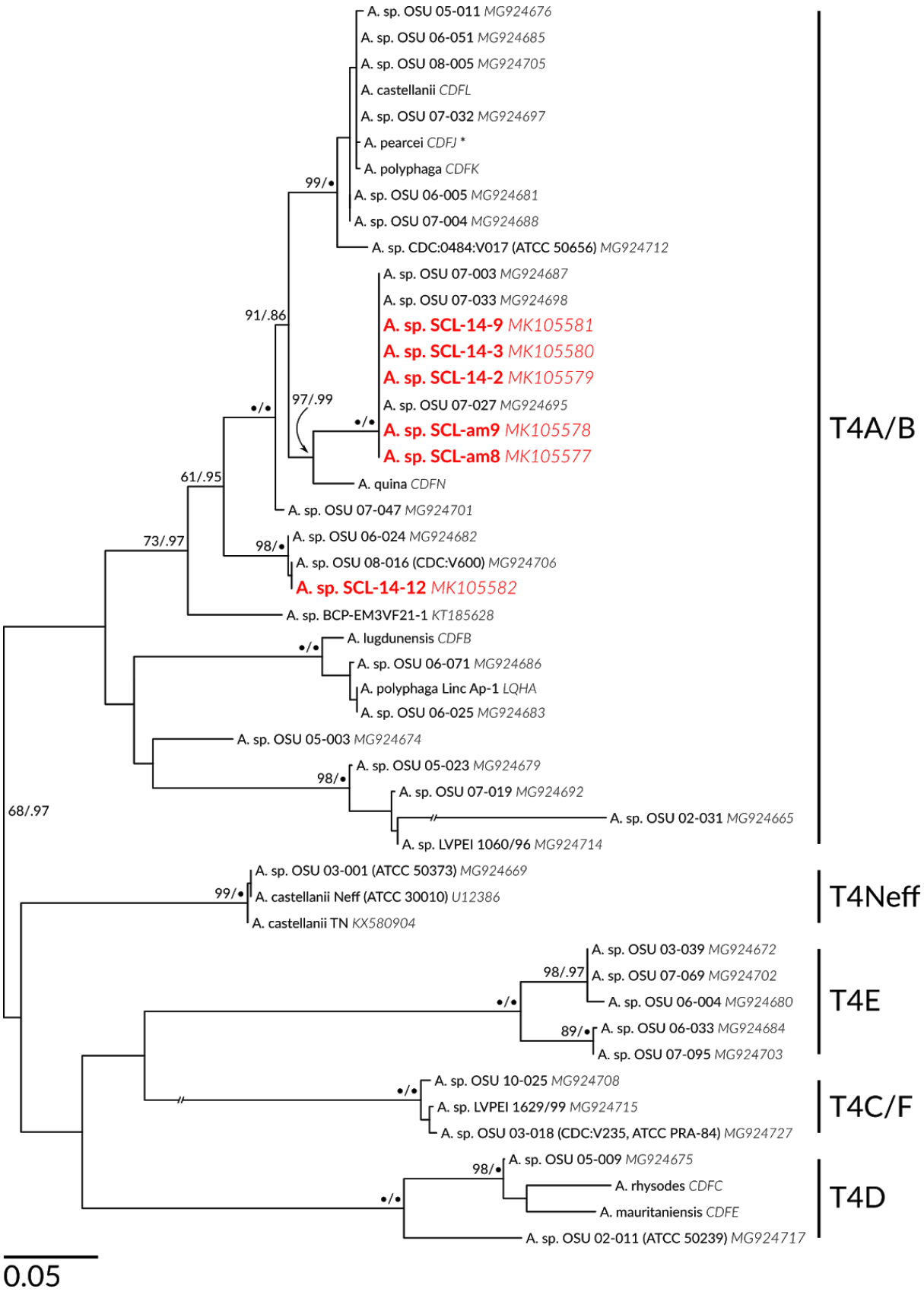

Figure 5 Cox1 ML-tree of *Acanthamoeba* T4 genotype rooted at midpoint. BA-tree gave the same topology. Branch supports are given as ML-bootstrap percentage / bayesian posterior probability. • – 100% or 1.00 support. * – Identification is dubious. Support values lower than 95/.75 are not shown.

Morphometrics

Trophozoites

The length of the measured trophozoites of all strains is between 15 and 47 µm, and the width between 5 and 27 µm (Fig 6, Tab 2). Locomotor forms of strain SCL-14-12 are considerably shorter (median 23 µm; $X^2(1, 5) = 92.765$, $p < 2.2\times10^{-16}$). The difference in length in all other strains is not significant. At the same time, the most narrow locomotor forms are those of strain SCL-am9 (median 12 µm; $X^2(1, 5) = 51.785$, $p = 5.971\times10^{-10}$). This leads to the significant difference in width-to-length ratio in the two strains, which is the biggest in SCL-14-12 (median 0.69) and the smallest in SCL-am9 (median 0.46) ($X^2(1, 5) = 72.762$, $p = 2.725\times10^{-14}$). This distinction in shape could be clearly observed by eye when inspecting a series of locomotor forms (Fig 1 A, B, C demonstrates the typical variants).

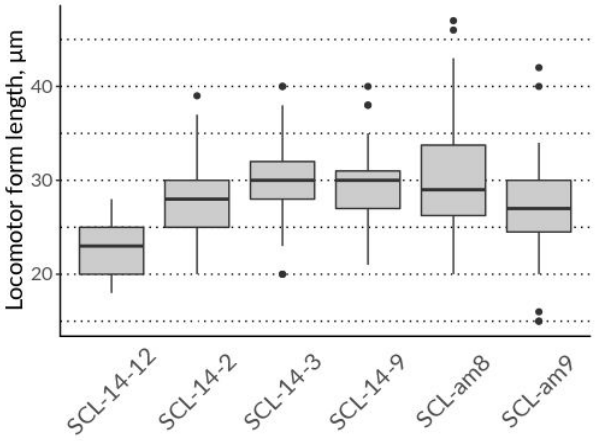

Figure 6 Locomotor form length in studied strains.

Table 2 Morphometric characteristics of locomotor forms of the studied strains. In braces is either a median absolute deviation (single number) or a range. **N** – number of measured individuals, **L** – length, **W** – width, **Round** – diameter of rounded cells, **NUC** – nucleus diameter, **nuc** – nucleolus diameter, **Hyal** – maximum breadth of the hyaline cap. All values except N and the ratios are in µm.

	SCL-14-12	**SCL-14-2**	**SCL-14-3**	**SCL-14-9**	**SCL-am8**	**SCL-am9**
N	55	55	55	55	54	57
L	23 (3.0)	28 (4.4)	30 (3.0)	30 (3.0)	29 (4.4)	27 (4.4)
W	15 (4.4)	17 (3.0)	16 (3.0)	15 (3.0)	15 (3.0)	12 (3.0)
W/L	0.69 (0.21)	0.60 (0.10)	0.56 (0.11)	0.50 (0.09)	0.51 (0.12)	0.46 (0.09)
Round	15	18	18	19	17	16
NUC	4 (3–6)	5 (4–7)	5 (4–7)	5 (4–6)	5 (3–9)	4 (3–6)
nuc	3 (2–3)	2 (2–3)	2 (2–3)	2 (2–3)	2 (1–3)	2 (1–3)

nuc/NUC	0.6 (0.1)	0.4 (0.1)	0.4 (0.1)	0.5 (0.1)	0.4 (0.1)	0.5 (0.1)
Hyal	4 (4–5)	6 (3–8)	7 (4–10)	5 (5–7)	6 (4–10)	6 (4–8)
Hyal/L	0.20 (0.03)	0.21 (0.03)	0.22 (0.03)	0.19 (0.03)	0.21 (0.05)	0.23 (0.06)

Some slight differences in the diameter of the nucleus and nucleolus have been observed. The median nucleus diameter in locomotor forms of strains SCL-14-12 and SCL-am9 (4 μm) are slightly lower than in other strains (5 μm) ($X^2(1, 5) = 62.971$, $p = 2.952\times10^{-12}$). The difference is marginally significant between SCL-14-12 and SCL-14-9, SCL-am9 and SCL-am8, and not significant between SCL-14-12 and SCL-am8. At the same time, the nucleolus in SCL-14-12 is significantly bigger (median diameter 3 μm) than in other strains (2 μm) ($X^2(1, 5) = 46.089$, $p = 8.712\times10^{-9}$). This results in significantly higher nucleolus-to-nucleus diameter ratio in strains SCL-14-12 and SCL-am9 (not different from SCL-14-9), and also partially in strain SCL-14-9. In strain SCL-14-12, the median of the hyaline crescent breadth is the lowest (4 μm) differing significantly from all other strains ($X^2(1, 5) = 128.58$, $p < 2.2\times10^{-16}$). Strain SCL-14-9 has the next lowest breadth, also differing significantly from other strains at 0.05 level.

Rounded cell diameter is between 15 μm in SCL-14-12 and 19 μm in SCL-14-9 and well correlates to the cell length (Spearman's $\rho = 0.87$, $S = 4.6324$, $p = 0.025$).

Cysts

Table 3 Morphometric characteristics of cysts and pseudocysts of the studied strains. Values In braces is a range. N – number of measured cysts, D – diameter (μm), Op – number of operculi.

		SCL-14-12	**SCL-14-2**	**SCL-14-3**	**SCL-14-9**	**SCL-am8**	**SCL-am9**
Cysts (bacterized culture)	**N**	82	82	82	80	84	80
	D	13 (10–15)	16 (13–22)	17 (13–23)	14 (11–21)	13 (10–16)	15 (11–20)
	Op	5 (3–6)	5 (4–9)	5 (4–8)	6 (4–10)	5 (2–7)	5 (3–8)
Cysts ("dense" culture)	**N**	55	111	85	87	79	100
	D	14 (11–16)	17 (13–20)	17 (15–22)	17 (14–22)	14 (10–18)	14 (10–18)
	Op	5 (4–7)	6 (3–7)	6 (4–9)	6 (4–9)	5 (3–7)	4 (2–6)
Cysts ("sparse" culture)	**N**	99	44	97	91	96	106
	D	15 (11–17)	18 (15–20)	19 (15–24)	19 (15–24)	17 (13–23)	16 (13–20)
	Op	6 (4–8)	5 (3–8)	6 (4–8)	7 (5–12)	5 (3–7)	4 (2–5)

We have found the cyst diameter a good character in terms of dispersion and inter-group differences. Not surprisingly, the dispersion of the cyst diameter in all estimated factor groups (“Strains” per “Culture type” design) is lower than that of the length and width in locomotor forms (MAD not greater than 12% of the median). The range of the measured cyst diameters is 10 to 24 µm (medians from 13 to 17 µm in bacterized cultures, from 14 to 17 µm in dense axenic cultures, and 15 to 19 µm in sparse axenic cultures) (Tab 3). Permutational analysis of variance shows the significance of the effect of “Strain” ($F(1, 5) = 263.6$, $p < .001$), “Culture type” ($F(1, 2) = 420.4$, $p < .001$), and their interaction ($F(1, 10) = 29.09$, $p < .001$). Generally, the cysts formed in bacterized cultures are the smallest followed by the cysts from dense axenic cultures and then by the cysts from sparse axenic cultures, which in all strains are about the same size than the “normal” rounded trophozoites (Fig 7), indicating almost no shrinkage during the cyst formation. In strains SCL-am8 and SCL-14-9, these differences in diameter are the most prominent, while SCL-14-12 has the smallest range (the difference is still significant).

No variation in the number of operculi is observed between cysts formed in different conditions.

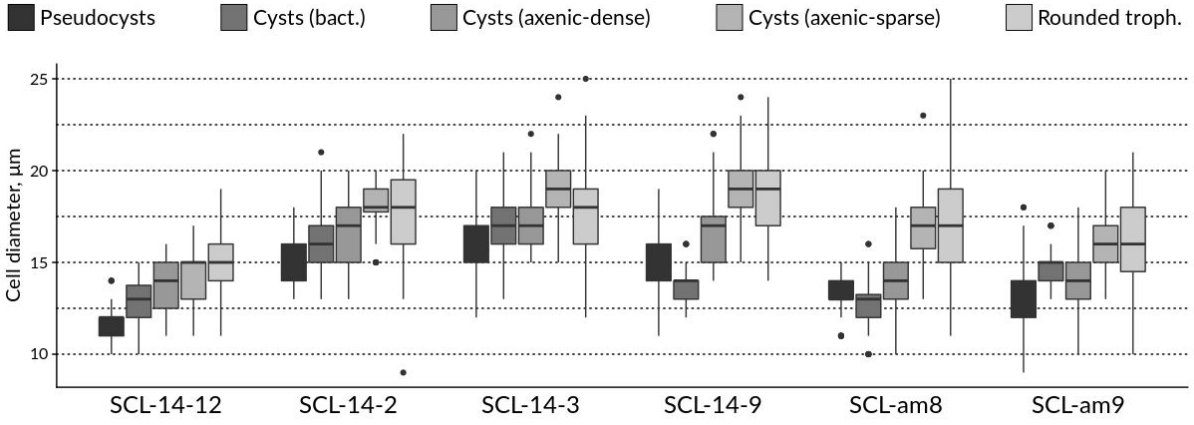

Figure 7 Diameter of rounded cell, cyst, and pseudocyst of the studied strains in different conditions

Pseudocysts

The diameter of the pseudocysts in the studied strains varies from 11 to 16 µm (Tab 4). As with cysts, SCL-14-12 is the smallest. Also, in all strains except SCL-14-9 and SCL-am8, pseudocysts are smaller than any type of cysts. In the two mentioned strains, cysts formed in bacterized cultures are slightly but significantly smaller than pseudocysts (Fig 7).

Table 4 Morphometric characteristics of pseudocysts of the studied strains. Values in braces are the range. **N** – number of measured pseudocysts, **D** – diameter (µm).

	SCL-14-12	SCL-14-2	SCL-14-3	SCL-14-9	SCL-am8	SCL-am9

N	52	52	57	55	56	51
D	11 (10–14)	15 (13–18)	15 (12–20)	14 (11–19)	13 (10–19)	13 (9–18)

Growth at different temperatures

The results of the preliminary test demonstrate that none of the isolated strains can maintain the stable growth at temperatures equal to or higher than 37°C, whether as axenic cultures in PYG medium or bacterized cultures on agar plates with WG medium overlay. At 40 and 42°C, cells die entirely in about a day. At 37°C, some cells remain alive for several days (more in bacterized than in axenic cultures), but their number declined to zero to the end of the week.

Table 5 Parameters of the logistic growth model at different temperatures. **L** – growth asymptote ($\times 10^6$ cell mL^{-1}); **k** – logistic growth rate.

		SCL-14-12	SCL-14-2	SCL-14-3	SCL-14-9	SCL-am8	SCL-am9
11°C	L	3.2	1.4	1.0	0.9	2.1	1.3
	k	0.01	0.01	0.01	0.01	0.01	0.02
18°C	L	3.2	0.7	0.6	1.3	1.8	1.3
	k	0.02	0.03	0.03	0.02	0.02	0.03
25°C	L	2.4	0.5	0.4	0.8	1.3	1.1
	k	0.02	0.03	0.05	0.04	0.03	0.03
32°C	L	1.4	0.5	0.4	0.9	0.8	0.1
	k	0.05	0.02	0.05	0.03	0.03	0.03

32°C is not favorable for all cultures, although at this temperature, they exhibit the fastest growth (Fig 8, Tab 5). In strains SCL-am8, SCL-am9, SCL-14-2, and SCL-14-3, cells do not attach to the substratum and always appear roundish. A typical monolayer has never been observed. Multinucleate cells start to appear from the first counting; subsequently, their amount and size increase. The population density curve reaches stationarity very quickly. The maximum culture density at this temperature does not exceed 8×10^5 cells mL^{-1} for SCL-am8, 5×10^5 cells mL^{-1} for SCL-14-2 and SCL-14-2, 2×10^5 cells mL^{-1} for SCL-am9. Strain SCL-14-12 attaches to the bottom and grows better than all in terms of the culture density (up to 2×10^6 cells mL^{-1} have been recorded), though this constitutes a considerable decrease compared to the densities at lower temperatures. Strain SCL-14-9 demonstrates a

behavior somewhat intermediate between SCL-14-12 and others. During the first two days, the culture grows well, and cells attach to the substratum. Later, most of them are found roundish and detached, and the monolayer is never formed. Multinucleate cells also appear, but later than in others and lower quantity. The density reaches 6×10^5 cells mL^{-1}.

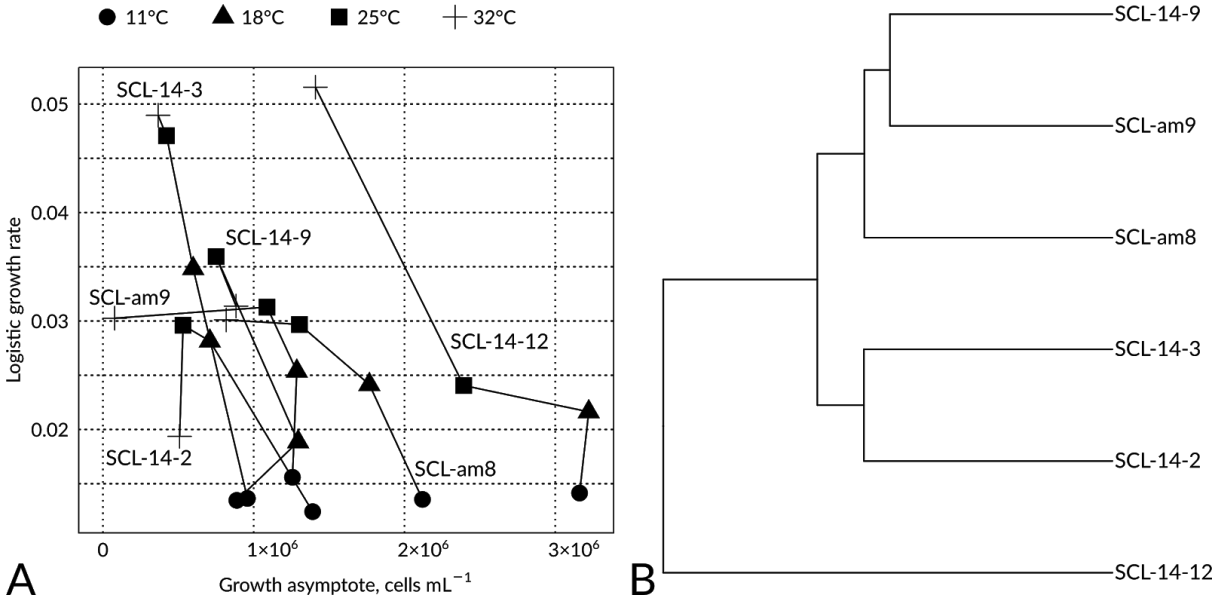

Figure 8 A – Scatter-plot representing modeled parameters of the logistic growth of the studied strains at different temperatures. Absciss – L, ordinate – k. Lines connect points belonging to the same strain. **B** – Cluster diagram of all three logistic model parameters (scaled). Euclidean distance, Ward's clustering method.

At 25°C, all strains grow well and form a monolayer in three to four days. Generally, the culture density increases faster than at 18°C but stops growing earlier, reaching the lower maximum. In strains SCL-am8, SCL-14-2, SCL-14-3 multinucleate cells also appear.

18°C is the optimal temperature for all strains. The maximal recorded densities are up to 8×10^5 cells mL^{-1} in SCL-14-2 and SCL-14-3; 1.5×10^6 cells mL^{-1} in SCL-am8, SCL-am9, and SCL-14-9; 2.8×10^6 cells mL^{-1} in SCL-14-12) since the active growth continues longer, although the growth rate is slightly lower than at 25°C. Cultures form a monolayer in four to seven days. Cells form pseudopodia and actively move during a long time, even at the stationary phase of growth.

At 11°C, all the cultures demonstrate a considerably lower rate of growth (Fig. 4). SCL-14-12 reaches a plateau in about 600 h at a density of more than 3×10^6 cells mL^{-1}. Other strains show similar dynamics and reach a plateau in 400 h at a density of about 1.5×10^6 cells mL^{-1} in SCL-am8 and about 1.0×10^6 cells mL^{-1} in others.

At 4°C, all the cultures have been in a good state during the whole period of observation, judging by the cell and overall culture appearance. However, counting

has shown that the cell number has been slightly declining, although dividing cells have been observed during the first two weeks.

The modeling of the logistic growth demonstrates three differences of SCL-14-12 in comparison to other strains. First, its density asymptote is higher than in other strains at any tested temperature, including 32°C. Second, its growth rate is about the same at 18 and 25°C, whereas in other strains, the growth rate at 25°C is considerably higher than at 18°C. Consequently, at 25°C, the growth rate of SCL-14-12 is lower than that of other strains. At the same time, at 32°C, the growth rate of SCL-14-12 is strikingly higher, while in others it is lower, the same, or (in SCL-14-3) just a little bit higher than at 25°C.

Discussion

Molecular phylogeny of *A. castellanii* complex (type T4)

18S

The distinctiveness of different clades inside type T4 has begun to manifest itself since the first works on *Acanthamoeba* rDNA diversity (Gast *et al.*, 1996; Stothard *et al.*, 1998; Chung *et al.*, 1998; Booton *et al.*, 2002; Kong, 2009; Fuerst *et al.*, 2015; Martín-Pérez *et al.*, 2017). Subtypes $T4_C$, $T4_D$, $T4_E$, $T4_F$, and $T4_{Neff}$, when represented by several sequences, were usually well-supported, while $T4_B$ was sometimes mixed with $T4_A$, and the latter mostly paraphyletic. At the same time, the relationship between the subtypes was never well-supported and appeared in part unstable. The deepest branching clade was either $T4_D$, $T4_E$, or a clade containing both of them. $T4_{Neff}$ appeared sister to either $T4_{A/B}$ or $T4_{D/E}$ mixed clades. $T4_{C/F}$ clade always branched after $T4_{D/E}$, except for the phylogeny using GTR model, where $T4_D$ was robustly sister to $T4_{A/B/Neff}$ cluster (Martín-Pérez et al., 2017).

In our case, automatic alignment with subsequent filtering yields robust clades (subtypes) $T4_C$ through $T4_{Neff}$, moderately supported $T4_B$, and paraphyletic $T4_A$ (tree not shown). All seven subtypes as monophyletic clades could only be obtained with Jukes-Cantor substitution model, the least-likely one in MrModelTest assessment. Relationships between the subtypes are poorly supported. However, the fifth-state-coding approach demonstrates the distinctiveness of all the T4 subtypes. The fact that $T4_C$—$T4_F$ subtypes may be obtained from the masked alignment demonstrates the adequateness of the fifth-state-coding method used. Moreover, monophyletic and fully-supported $T4_B$, $T4_D$—$T4_F$, and $T4_{Neff}$ may also be obtained using the alignment of conservative regions only.

Thus, our 18S phylogeny corroborates and validates the previously obtained results. At the same time, the method bears some possible sources of bias: (i) Indels of more than one nucleotide are treated as separate events, while they may actually represent a single event, (ii) Inversions are treated as several events, (iii) The amount of transversions is probably underestimated, (iv) Unresolvable position of indels in single-nucleotide repeats. This probable bias may explain differences in topology between BA and ML trees.

16S

As demonstrated by Ledee et al. (2003), 16S and 18S-based phylogenies of *Acanthamoeba* corroborate each other in terms of identified sequence types. This holds for T4 type as well. Also, even an early mitochondrial RFLP study (Byers, Bogler, & Burianek, 1983) has revealed remarkable heterogeneity inside 16S-T4 comparable to that found in 18S-T4. At the same time, this study has discovered the major inconsistency between 18S and 16S phylogenies: Castellani and Ma strains (18S-$T4_A$ and $T4_B$, correspondingly) appeared closely related and showed differences at the level of intraspecific variation in other organisms. Other 18S-T4 type strains included in this study, namely Neff, Singh, and Page-23, were found to be as distant as other types.

The sequence-based 16S phylogeny (Ledee *et al.*, 2003) demonstrated the identity of Castellani and Ma (as well as CDC:V042) sequences. Here, about 15% bases were removed as ambiguously aligned, which explains why differences found by Byers et al. (1983) were not observed. The rest of the sequences attributed to 18S-$T4_A$ and $T4_B$ subtypes were intermixed. Nine new clades were identified inside 16S-T4. Sequences of the strains attributed to 18S subtypes $T4_C$, $T4_D$, $T4_E$, $T4_{Neff}$ formed corresponding clades on the 16S tree ($T4_F$ sequences were not included). The deepest branching clade was $T4_E$ following by $T4_C$, then $T4_{Neff}$ clade. $T4_D$ sequences formed a clade sister to mixed $T4_{A/B}$ clade. Kong (2009) using a smaller dataset identified five 16S clades, namely the deepest branching $T4_C$, the next branching $T4_D$, then $T4_{Neff}$, and the last branching $T4_{A/B}$, which in turn consisted of two clusters: the one containing, among others, Ma and Castellani strains and another one containing *A. lugdunensis* L3a. Finally, Rahman et al. (2013) adding 13 T4 rns sequences obtained generally the same nine clades as Ledee et al. (2003) inside T4 subtype.

We have identified around 13 well-supported clusters inside rns-T4 subtype. In addition to the proximity of Castellani and Ma strains, our study reveals other discrepancies between the 18S and 16S phylogenies. Permafrost strains SCL-am9 and SCL-14-9 belonging to 18S-$T4_A$ subtype and SCL-am8, SCL-14-2, SCL-14-3, belonging to 18S-$T4_B$ subtype, all have identical 16S sequences (even before masking). Strains CDC:V042 (ATCC 50493) and CDC:V390 get into same “Rawdon”

clade in 18S tree, but appear all distant in 16S tree. Strain CDC:V042 is close to Castellani strain while being placed in a different highly supported subcluster of $T4_A$ by 18S phylogeny. Galka strain (ATCC 50496) groups together with SCL-am9 on the 18S tree, but is steadily apart from it on the 16S tree. By contrast, strain CDC:V390 robustly branches apart from Galka on the 18S tree but has identical 16S sequence. At the same time, strain Liu-E1 (ATCC 50709) is close to Galka in terms of 18S, and 16S sequences of these two strains are identical too. Strain SCL-14-12, which robustly clusters together with Castellani strain in absolutely all 18S analyses, steadily falls apart from it on the 16S tree. Finally, strains Rawdon (BCM:37, ATCC 50497) and CDC:V390 cluster together with high support on the 18S tree, but are steadily apart on the 16S tree.

To summarize, some of the strains demonstrate proximity in terms of 18S sequence but are distant in terms of 16S sequence, some are close in terms of 16S, but have distant 18S sequences, and other ones appear closely related in both phylogenies.

To explain such complex dissimilarity between 18S and 16S phylogenies, three hypotheses may be involved. The first implies different rates of gene evolution in different strains, which is unlikely regarding their taxonomic proximity. As the second, the improper alignment of indels may be invoked (see the consideration of possible sources of bias above). Indeed, in single-nucleotide stretches in an alignment, indels may occur in any position and ideally should not be aligned (which is nonetheless done for the sake of parsimony). When indels are treated as the fifth state and included in the calculation, their alignment may force sequences to appear more similar than they are. This possibility cannot be completely ruled out here, but against it is the fact that only A and B and C and F 18S subtypes became intermingled in 16S tree, while the others (D, E, and Neff) stayed separate. Also, this hypothesis may explain why sequences that are close to each other in 18S phylogeny appear distant in 16S one, but not the opposite cases (as our 16S phylogeny did not account for indels).

The third hypothesis maintains that 18S subtypes $T4_A$ and $T4_B$, as well as $T4_C$ and $T4_F$, actually represent intra-genomic variants of the gene present in the cell in a different number of copies, with only the dominant one revealed by the PCR. Different strains may bear different dominant variants and thus be attributed to either A or B (C or F) subtype while sharing the same (or closely related) 16S gene sequences. Intragenomic variation in 18S gene sequence is known in different protist supergroups including other Amoebozoa (Amaral-Zettler *et al.*, 2006; Gribble & Anderson, 2007; Nassonova *et al.*, 2010; Pillet, Fontaine, & Pawlowski, 2012; Gong *et al.*, 2013; Kudryavtsev & Gladkikh, 2017; Ntakou *et al.*, 2019) and reported for several *Acanthamoeba* strains (Stothard *et al.*, 1998; Nuprasert *et al.*, 2010; Qvarnstrom, Nerad, & Visvesvara, 2013; Rahman *et al.*, 2013). Furthermore, among 18S intragenomic variants found by Rahman et al. (2013) in two strains, one belongs

to $T4_A$ and another to $T4_B$ (the alignment is available upon request). Also, this hypothesis may explain common difficulties with obtaining a full 18S sequence from *Acanthamoeba* strains (the picture of contamination in chromatograms from a clonal culture) and rarely reported cases when different 18S variants were obtained from the same lens of a patient (Booton *et al.*, 2002); $T4_A$ and $T4_C$) or from the right and left lens cases (Ledee *et al.*, 2009); both $T4_B$).

Cox1

The strains for which Cox1 sequences are available mostly have no full 18S sequences in the public domain. Our Cox1 phylogeny fully corroborated the 16S phylogeny in the proximity of 18S-$T4_{A/B}$, as well as 18S-$T4_{C/F}$, strains, the distinctiveness of other subtypes, and the internal heterogeneity of $T4_{A/B}$ clade. Here again, strain SCL-14-12 was firmly placed into different cluster than all other permafrost strains, which suggests the correspondence of the Cox1 clusters to the 16S ones.

Morphometrics

Traditional taxonomy of *Acanthamoeba* has been primarily based on metric (overall diameter, nucleus diameter, nucleolus diameter) and meristic (number of “angles”, or “corners”, or “arms”, i.e. protrusions of endocyst towards operculi) characters of cysts since Page’s redescription of *A. castellanii*, *A. polyphaga*, and *Acanthamoeba astronyxis* (Page, 1967). Pussard and Pons emphasized the number of angles and properties of endo- and ectocyst (smoothness, distinctiveness), which they have studied in a considerable amount of strains using different staining techniques (Pussard & Pons, 1977). However, with the number of strains growing, the variability in these characters also grew and has become overlapping. Also, as a rule, no statistical comparison of studied characters has been conducted those times, although the number of measured individuals was usually sufficient. The use of molecular methods has shown striking similarity of some of the described species, e.g., *Acanthamoeba terricola* Pussard, 1964 and *A. castellanii* Neff strain (Visvesvara & Balamuth, 1975); *Acanthamoeba divionensis* Pussard et Pons, 1977, *Acanthamoeba paradivionensis* Pussard et Pons, 1977, *Acanthamoeba mauritaniensis* Pussard et Pons, 1977, and *Acanthamoeba rhysodes* Singh, 1952 (De Jonckheere, 1983; Liu *et al.*, 2005). Since the beginning of the DNA sequencing era, the attention of investigators has been concentrated on molecular phylogeny, and little attempts have been made to correspond morphometric features to molecular clusters. As a result, no integrated species concept for *Acanthamoeba* that would include both molecular and morphological characters seems to exist by now.

All our strains exhibit differences in the measured morphometric characters. The morphometrics of locomotor forms demonstrates the relative stability of metric

characters. For the width, the most variable trait, the median absolute deviation (MAD) is in the range from 17.4% (SCL-14-2) to 29.7% (SCL-am8) of the median (standard deviation (SD) from 16.5% to 25.5%). The MAD of the length is between 9.9% (SCL-14-3 and SCL-14-9) and 16.5% (SCL-am9) of the median (SD 12.1% to 19.4%). The level of variability found in the measured characters of cysts is even lower (not surprisingly). With the number of measured cells around 50, this level of variability allow to register significant differences (at $p \leq .05$) even between genetically closely related strains (Tab 2, 3).

It should be stressed, that culture conditions among strains during the measurement taking were held essentially the same to assure that the observed differences may be attributed to genotypes. Unsurprisingly, we have found significant variability associated with the type and density of the culture in cysts (Tab 3, Fig 7). This indicates that the obtained results are valid for the comparison of the studied strains but may not be used to compare with literature data unless the conditions of culturing coincide exactly.

The classifications of the strains based upon different subsets of the morphometric data demonstrates different levels of similarity with molecular classification (Fig 9). As it was discussed previously, five out of six strains are identical in mitochondrial gene sequences, so the only topological feature shared by all molecular trees is the most distant position of SCL-14-12. Not all morphological trees share this feature as well. Specifically, this is the case for locomotor form and sparse axenic cyst measurements (Fig 9F, G), which also drives the overall configuration (Fig 9D). The dense axenic cyst and bacterized cyst data (Fig 9H, I), as well as the pseudocyst data, do not show this topology. Notably, monoclonal bacterized culture on an agar plate is the most common setting in which measurements have been taken from different *Acanthamoeba* strains, partially because not in every case a culture has been axenized, and partially because this has been (probably rightly) believed to most closely resemble the natural conditions. Our results suggest that measurements taken in axenic conditions may better reflect genetic differences.

Thus, the most distant position of strain SCL-14-12 is not absolutely stable when different sets of features and different culture conditions are compared. At the same time, we tend to attach greater importance to the measurements of locomotor forms as to embracing more different cell features. In addition to significant differences in linear dimensions, strain SCL-14-12 also differs from others by its proportions, specifically the width to length, nucleolus to nucleus diameter, and hyaloplasm width to cell length ratios. It should be noted that not only SCL-14-12 is the most distant strain in the locomotor form-based classification, but also the further branching (SCL-am9, then SCL-14-9) partially follows the order of the 18S tree (Fig 9C).

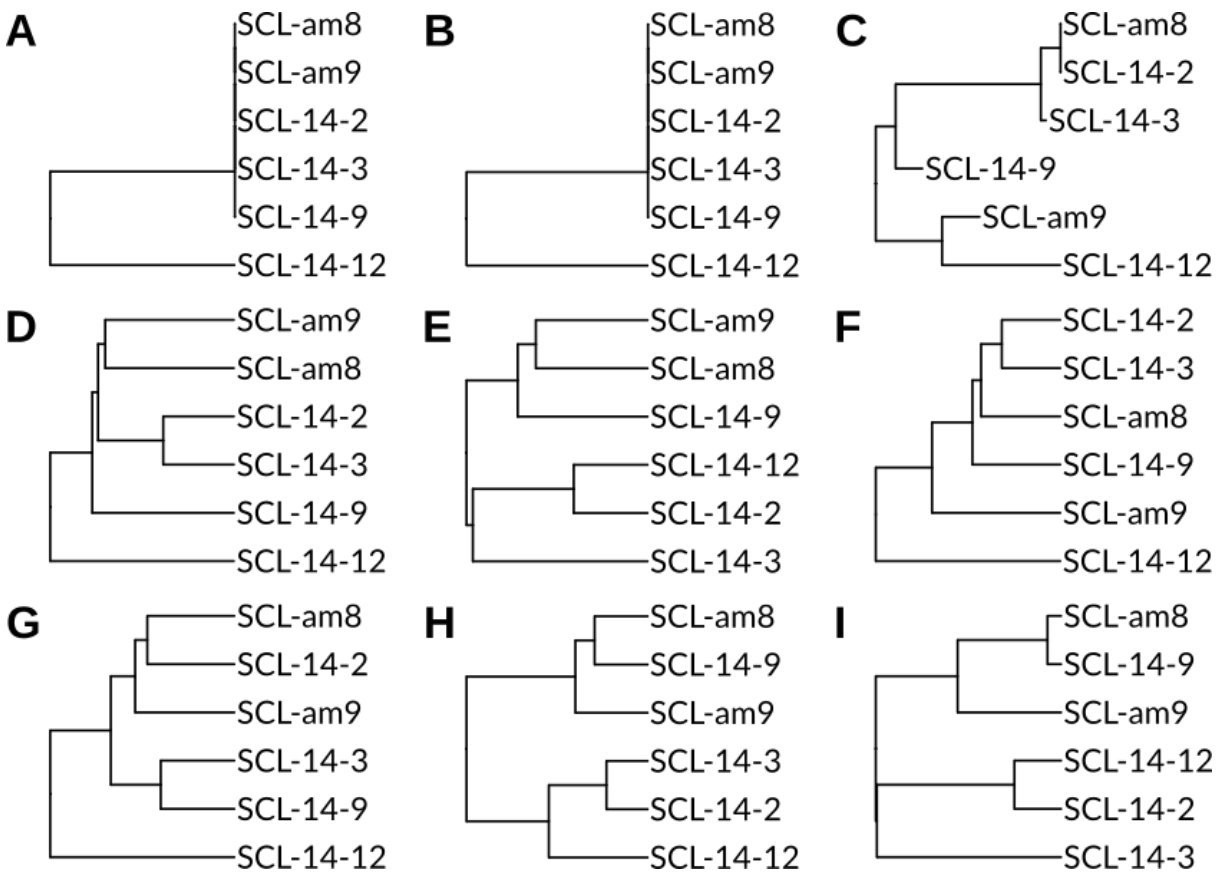

Figure 9 Classification of the strains based on different data. **Gene trees: A** – Cox1 NJ tree, observed distances; **B** – 16S NJ tree, observed distances; **C** – 18S tree extracted from the complete tree of T4 type. **Morphometric trees: D** – All features included; **E** – Cysts and pseudocysts only; **F** – Trophozoites only; **G** – "Sparse" axenic cysts; **H** – "Dense" axenic cysts; **I** – Bacterized culture cysts. All trees are rooted at midpoint. Not to scale.

So, to reliably compare morphometric data between strains in *Acanthamoeba* (and other amoebae), the establishment of standardized culture conditions is absolutely necessary. The axenic culture in a defined medium is the best candidate for such a standard, but the temperature should obviously be considered as well.

Growth at different temperatures

As with the morphometric data, we observe differences in the culture growth are between all studied strains and temperatures. Generally, the higher the temperature, the higher the logistic growth rate, and the lower the culture density asymptote. Also, at temperatures from 25°C and higher, multinucleate cells appear, prevailing over the normal mononucleate cells at 32°C in most strains. James and Byers (1967) also observed multinucleates in aging cultures; their amount was increased by agitation or air bubbling. Corsaro et al. (2015) observed multinucleates in a culture of *Acanthamoeba micheli* Corsaro, Walochnik, Köhsler et Rott, 2015. Most likely, multinucleate cells result from incomplete cell division (karyokinesis not followed by

cytokinesis), but the possibility of cell fusion also cannot be ruled out (Pigon, 1972). Our data strongly supports the first way.

In the growth data, strain SCL-14-12 is also obviously different from others. At 25°C, it shows approximately the same growth rate as at 18°C, while other strains increase it. At 32°C, no multinucleate cells appear in this strain, and the cells are attached to the substratum. Also, the growth rate is the highest. Thus, in addition to higher growth limits at all temperatures tested (a feature stemming probably from its smaller size), SCL-14-12 is characterized by a broader range of temperatures suitable for normal culture growth.

The potential pathogenicity of *Acanthamoeba* strains is often addressed by testing their possibility to grow at 34°C, a temperature of the human cornea (Walochnik, Obwaller, & Aspöck, 2000), and 37°C. All permafrost strains except SCL-14-12 demonstrate clear signs of dysfunction already at 32°C, and may thus be considered non-pathogenic. For SCL-14-12, the potential to cause keratitis cannot be excluded.

Conclusion

Although a complex comparative study of strains inside *A. castellanii* complex (ribotype T4) remains a future perspective, our investigation demonstrates that the results of consistently applied morphometrics and ecophysiological studies (characteristics of growth at different temperatures) are in line with molecular variability of several kinds of genes (nuclear and mitochondrial) and may thus form a basis for *Acanthamoeba*-specific species concept. Amid the diversity of the entire genus, all studied strains are closely related to each other. However, strain SCL-14-12 is unique in all three sequenced genes, while the others possess the same sequences of the mitochondrial genes. Phylogenies built with all available sequences firmly place SCL-14-12 apart from the other strains. At the same time, it differs by many morphometric characters of both trophozoites and cysts, including proportions, as well as growth characteristics at different temperatures. Besides, directly observable features of cultures also distinguish this strain from the others. Other strains also exhibit some variation (and are obviously different in their 18S sequences), but this variation does not involve all studied features and is smaller in magnitude. Taking all this into account, we consider strain SCL-14-12 and other permafrost strains as two separate species. This conclusion may also be extrapolated onto other clusters obtained in mitochondrial phylogenies inside $T4_{A/B}$ clade, if only morphological and ecophysiological differences of strains between those clusters are consistent, which needs further investigation. Until such investigation placing phenotypic divergence in the framework of steady multigene phylogeny is done, a revision of *A. castellanii* species complex and thus the genus as a whole seems not possible.

Although most of *Acanthamoeba* 18S rDNA types are conceivably real taxa, in *A. castellanii* complex the phylogenetic signal of this gene is biased, and thus it should not be used for species delimitation in this group. Mitochondrial gene phylogenies seem to be more suitable for this purpose.

Acknowledgements

This study partially utilized microscopy equipment of the Core Facility Centres “Development of molecular and cell technologies” and “Culture Collection of Microorganisms” of Saint Petersburg State University (SPSU). We thank Dr. Alexei Smirnov for providing the possibility to use these facilities. We are obliged to all Soil Cryology lab members who participated in field sampling. We would also like to thank Prof. Dr. Jean-Michel Claverie, Laboratoire Information Génomique et Structurale, Aix Marseille Université, for his valuable comments on the manuscript.

This study was conducted in the framework of the Governmental Program 0191-2019-0044 and supported by Russian Foundation for Basic Research (RFBR) grants 18-04-00824 (isolation and culture establishment) and 17-54-150003 (description of the strains).

References

Amaral-Zettler LA, Cole J, Laatsch AD, Nerad TA, Anderson OR, Reysenbach AL. 2006. Vannella epipetala n. sp. Isolated from the Leaf Surface of Spondias mombin (Anacardiaceae) Growing in the Dry Forest of Costa Rica. *The Journal of Eukaryotic Microbiology* 53: 522–530.
Boenigk J, Ereshefsky M, Hoef-Emden K, Mallet J, Bass D. 2012. Concepts in protistology: Species definitions and boundaries. *European Journal of Protistology* 48: 96–102.
Booton GC, Joslin CE, Shoff M, Tu EY, Kelly DJ, Fuerst PA. 2009. Genotypic Identification of Acanthamoeba sp. Isolates Associated with an Outbreak of Acanthamoeba keratitis (AK). *Cornea* 28: 673–676.
Booton GC, Kelly DJ, Chu YW, Seal DV, Houang E, Lam DSC, Byers TJ, Fuerst PA. 2002. 18S Ribosomal DNA Typing and Tracking of Acanthamoeba Species Isolates from Corneal Scrape Specimens, Contact Lenses, Lens Cases, and Home Water Supplies of Acanthamoeba Keratitis Patients in Hong Kong. *Journal of Clinical Microbiology* 40: 1621–1625.
Booton GC, Kelly DJ, Fuerst PA. 2005. Genotypic identification and species names in Acanthamoeba: correlation and conflict. *The Journal of Eukaryotic Microbiology* 52: 7S-27S.
Byers TJ, Bogler SA, Burianek LL. 1983. Analysis of Mitochondrial DNA Variation as an Approach to Systematic Relationships in the Genus Acanthamoeba1. *The Journal of Protozoology* 30: 198–203.
Chung DI, Yu HS, Hwang MY, Kim TH, Kim TO, Yun HC, Kong HH. 1998. Subgenus classification of Acanthamoeba by riboprinting. *The Korean Journal of Parasitology*

36: 69–80.
Clarke M, Lohan AJ, Liu B, Lagkouvardos I, Roy S, Zafar N, Bertelli C, Schilde C, Kianianmomeni A, Bürglin TR, others. 2013. Genome of Acanthamoeba castellanii highlights extensive lateral gene transfer and early evolution of tyrosine kinase signaling. *Genome biology* 14: R11.
Corsaro D, Köhsler M, Montalbano Di Filippo M, Venditti D, Monno R, Di Cave D, Berrilli F, Walochnik J. 2017. Update on Acanthamoeba jacobsi genotype T15, including full-length 18S rDNA molecular phylogeny. *Parasitology Research* 116: 1273–1284.
Corsaro D, Venditti D. 2018. An apparent Acanthamoeba genotype is the product of a chimeric 18S rDNA artifact. *Parasitology Research* 117: 571–577.
Corsaro D, Walochnik J, Köhsler M, Rott MB. 2015. Acanthamoeba misidentification and multiple labels: redefining genotypes T16, T19, and T20 and proposal for Acanthamoeba micheli sp. nov. (genotype T19). *Parasitology Research* 114: 2481–2490.
De Jonckheere JF. 1983. Isoenzyme and Total Protein Analysis by Agarose Isoelectric Focusing, and Taxonomy of the Genus Acanthamoeba. *The Journal of Protozoology* 30: 701–706.
Demidov NE, Baranskaya AV, Durdenko EV, Zanina OG, Karaevskaya ES, Pushina ZV, Rivkina EM, Spirina EV, Spenser R. 2016. [Biogeochemistry of the permafrost of the Arctic coast of the Gydan Peninsula]. *Problems of the Arctic and Antarctic* 3: 34–49.
Elzhov TV, Mullen KM, Spiess AN, Bolker B. 2016. *minpack.lm: R Interface to the Levenberg-Marquardt Nonlinear Least-Squares Algorithm Found in MINPACK, Plus Support for Bounds*.
Fuerst PA. 2014. Insights from the DNA databases: Approaches to the phylogenetic structure of Acanthamoeba. *Experimental Parasitology* 145: S39–S45.
Fuerst PA, Booton GC, Crary M. 2015. Phylogenetic Analysis and the Evolution of the 18S rRNA Gene Typing System of Acanthamoeba. *Journal of Eukaryotic Microbiology* 62: 69–84.
Gast RJ, Ledee DR, Fuerst PA, Byers TJ. 1996. Subgenus systematics of Acanthamoeba: four nuclear 18S rDNA sequence types. *Journal of Eukaryotic Microbiology* 43: 498–504.
Gast RJ, Moran DM, Dennett MR, Wurtsbaugh WA, Amaral- Zettler LA. 2011. Amoebae and Legionella pneumophila in saline environments. *Journal of water and health* 9: 37–52.
Geisen S, Fiore-Donno AM, Walochnik J, Bonkowski M. 2014. Acanthamoeba everywhere: high diversity of Acanthamoeba in soils. *Parasitology Research* 113: 3151–3158.
Gilichinskiy DA, Khlebnikova GM, Zvyagintsev DG, Fedorov-Davydov DG, Kudryavtseva NN. 1989. Microbiology of sedimentary materials in the permafrost zone. *International Geology Review* 31: 847–858.
Gilichinsky DA, Rivkina EM. 2011a. Permafrost microbiology. In: Reitner J,, In: Thiel V, eds. *Encyclopedia of Earth Sciences Series*. *Encyclopedia of Geobiology*. Springer Netherlands, 726–732.
Gilichinsky DA, Rivkina EM. 2011b. Permafrost microbiology. In: Reitner J,, In: Thiel V, eds. *Encyclopedia of Earth Sciences Series*. *Encyclopedia of Geobiology*. Springer Netherlands, 726–732.

Gong J, Dong J, Liu X, Massana R. 2013. Extremely High Copy Numbers and Polymorphisms of the rDNA Operon Estimated from Single Cell Analysis of Oligotrich and Peritrich Ciliates. *Protist* 164: 369–379.
Gribble KE, Anderson DM. 2007. High intraindividual, intraspecific, and interspecific variability in large-subunit ribosomal DNA in the heterotrophic dinoflagellates Protoperidinium, Diplopsalis, and Preperidinium (Dinophyceae). *Phycologia* 46: 315–324.
Gunderson JH, Sogin ML. 1986. Length variation in eukaryotic rRNAs: small subunit rRNAs from the protists Acanthamoeba castellanii and Euglena gracilis. *Gene* 44: 63–70.
James TE, Byers TJ. 1967. The induction of multinuclearity in agitated and in aging cultures of Acanthamoeba sp. Neff. *Journal of Cellular Physiology* 70: 53–61.
Juck DF, Whissell G, Steven B, Pollard W, McKay CP, Greer CW, Whyte LG. 2005. Utilization of Fluorescent Microspheres and a Green Fluorescent Protein-Marked Strain for Assessment of Microbiological Contamination of Permafrost and Ground Ice Core Samples from the Canadian High Arctic. *Applied and Environmental Microbiology* 71: 1035–1041.
Katoh K, Standley DM. 2013. MAFFT Multiple Sequence Alignment Software Version 7: Improvements in Performance and Usability. *Molecular Biology and Evolution* 30: 772–780.
Khan NA. 2005. Granulomatous Amoebic Encephalitis: Clinical Diagnosis and Management. *American Journal of Infectious Diseases* 1: 79–83.
Kliescikova J, Kulda J, Nohynkova E. 2011. Stress-Induced Pseudocyst Formation - A Newly Identified Mechanism of Protection against Organic Solvents in Acanthamoebae of the T4 Genotype. *Protist* 162: 58–69.
Kochkina G, Ivanushkina N, Ozerskaya S, Chigineva N, Vasilenko O, Firsov S, Spirina E, Gilichinsky D. 2012. Ancient fungi in Antarctic permafrost environments. *FEMS Microbiology Ecology* 82: 501–509.
Kong HH. 2009. Molecular Phylogeny of Acanthamoeba. *The Korean Journal of Parasitology* 47: S21–S28.
Kudryavtsev A, Gladkikh A. 2017. Two new species of Ripella (Amoebozoa, Vannellida) and unusual intragenomic variability in the SSU rRNA gene of this genus. *European Journal of Protistology* 61: 92–106.
Ledee DR, Booton GC, Awwad MH, Sharma S, Aggarwal RK, Niszl IA, Markus MB, Fuerst PA, Byers TJ. 2003. Advantages of Using Mitochondrial 16S rDNA Sequences to Classify Clinical Isolates of Acanthamoeba. *Investigative Opthalmology & Visual Science* 44: 1142.
Ledee DR, Iovieno A, Miller D, Mandal N, Diaz M, Fell J, Fini ME, Alfonso EC. 2009. Molecular Identification of T4 and T5 Genotypes in Isolates from Acanthamoeba Keratitis Patients. *Journal of Clinical Microbiology* 47: 1458–1462.
Legendre M, Bartoli J, Shmakova L, Jeudy S, Labadie K, Adrait A, Lescot M, Poirot O, Bertaux L, Bruley C, others. 2014. Thirty-thousand-year-old distant relative of giant icosahedral DNA viruses with a pandoravirus morphology. *Proceedings of the National Academy of Sciences* 111: 4274–4279.
Liu H, Ha YR, Lee ST, Hong YC, Kong HH, Chung DI. 2006. Genetic diversity of Acanthamoeba isolates from ocean sediments. *The Korean journal of parasitology* 44: 117.
Liu H, Moon EK, Yu HS, Jeong HJ, Hong YC, Kong HH, Chung DI. 2005. Evaluation

of taxonomic validity of four species of Acanthamoeba: A. divionensis, A. paradivionensis, A. mauritaniensis, and A. rhysodes, inferred from molecular analyses. *The Korean Journal of Parasitology* 43: 7–13.
Maciver SK, Asif M, Simmen MW, Lorenzo-Morales J. 2013. A systematic analysis of Acanthamoeba genotype frequency correlated with source and pathogenicity: T4 is confirmed as a pathogen-rich genotype. *European Journal of Protistology* 49: 217–221.
Martín-Pérez T, Criado-Fornelio A, Martínez J, Blanco MA, Fuentes I, Pérez-Serrano J. 2017. Isolation and molecular characterization of Acanthamoeba from patients with keratitis in Spain. *European Journal of Protistology* 61: 244–252.
Maycock NJR, Jayaswal R. 2016. Update on Acanthamoeba Keratitis: Diagnosis, Treatment, and Outcomes. *Cornea* 35: 713.
Megha K, Sharma M, Gupta A, Sehgal R, Khurana S. 2018. Protein profiling of Acanthamoeba species using MALDI-TOF MS for specific identification of Acanthamoeba genotype. *Parasitology Research* 117: 729–736.
Nassonova E, Smirnov A, Fahrni J, Pawlowski J. 2010. Barcoding Amoebae: Comparison of SSU, ITS and COI Genes as Tools for Molecular Identification of Naked Lobose Amoebae. *Protist* 161: 102–115.
Neff RJ, Ray SA, Benton WF, Wilborn M. 1964. Induction of synchronous encystment (differentiation) in Acanthamoeba sp. *Methods in Cell Biology*.55–83.
Nguyen LT, Schmidt HA, von Haeseler A, Minh BQ. 2015. IQ-TREE: A Fast and Effective Stochastic Algorithm for Estimating Maximum-Likelihood Phylogenies. *Molecular Biology and Evolution* 32: 268–274.
Ntakou E, Siemensma F, Bonkowski M, Dumack K. 2019. The Dancing Star: Reinvestigation of Artodiscus saltans (Variosea, Amoebozoa) Penard 1890. *Protist*: S1434461018301251.
Nuprasert W, Putaporntip C, Pariyakanok L, Jongwutiwes S. 2010. Identification of a Novel T17 Genotype of Acanthamoeba from Environmental Isolates and T10 Genotype Causing Keratitis in Thailand. *Journal of Clinical Microbiology* 48: 4636–4640.
Oksanen J, Blanchet FG, Friendly M, Kindt R, Legendre P, McGlinn D, Minchin PR, O'Hara RB, Simpson GL, Solymos P, Stevens MHH, Szoecs E, Wagner H. 2019. *vegan: Community Ecology Package*.
Page FC. 1967. Re-Definition of the Genus Acanthamoeba with Descriptions of Three Species. *The Journal of Protozoology* 14: 709–724.
Page FC. 1988. *A new key to freshwater and soil gymnamoebae: with instructions for culture*.
Pigon A. 1972. Inhibition of movement, attachment, and cytokinesis by autogenous substances in the amoeba Hartmannella. *Experimental Cell Research* 73: 170–176.
Pillet L, Fontaine D, Pawlowski J. 2012. Intra-Genomic Ribosomal RNA Polymorphism and Morphological Variation in Elphidium macellum Suggests Inter-Specific Hybridization in Foraminifera. *PLOS ONE* 7: e32373.
Pussard M, Pons R. 1977. Morphologie de la paroi kystique et taxonomie du genre Acanthamoeba (Protozoa, Amoebida). *Protistologica* 13: 557–598.
Qvarnstrom Y, Nerad TA, Visvesvara GS. 2013. Characterization of a New Pathogenic Acanthamoeba Species, A. byersi n. sp., Isolated from a Human with Fatal Amoebic Encephalitis. *The Journal of eukaryotic microbiology* 60: 626–633.
R Core Team. 2019. *R: A Language and Environment for Statistical Computing*.

Vienna, Austria: R Foundation for Statistical Computing.
Rahman MM, Yagita K, Kobayashi A, Oikawa Y, Hussein AIA, Matsumura T, Tokoro M. 2013. Genetic Characterization of Clinical Acanthamoeba Isolates from Japan using Nuclear and Mitochondrial Small Subunit Ribosomal RNA. *The Korean Journal of Parasitology* 51: 401–411.
Rivkina EM, Friedmann EI, McKay CP, Gilichinsky DA. 2000. Metabolic activity of permafrost bacteria below the freezing point. *Applied and Environmental Microbiology* 66: 3230–3233.
Ronquist F, Teslenko M, van der Mark P, Ayres DL, Darling A, Höhna S, Larget B, Liu L, Suchard MA, Huelsenbeck JP. 2012. MrBayes 3.2: Efficient Bayesian phylogenetic inference and model choice across a large model space. *Syst. Biol.* 61: 539–542.
Schirrmeister L, Kunitsky V, Grosse G, Wetterich S, Meyer H, Schwamborn G, Babiy O, Derevyagin A, Siegert C. 2011. Sedimentary characteristics and origin of the Late Pleistocene Ice Complex on north-east Siberian Arctic coastal lowlands and islands – A review. *Quaternary International* 241: 3–25.
Shatilovich AV, Shmakova LA, Mylnikov AP, Gilichinsky DA. 2009. Ancient Protozoa Isolated from Permafrost. In: Margesin R, ed. *Permafrost Soils*. Berlin, Heidelberg: Springer Berlin Heidelberg, 97–115.
Shatilovich A, Stoupin D, Rivkina E. 2015. Ciliates from ancient permafrost: Assessment of cold resistance of the resting cysts. *European Journal of Protistology* 51: 230–240.
Shatilovich AV, Tchesunov AV, Neretina TV, Grabarnik IP, Gubin SV, Vishnivetskaya TA, Onstott TC, Rivkina EM. 2018. Viable Nematodes from Late Pleistocene Permafrost of the Kolyma River Lowland. *Doklady Biological Sciences* 480: 100–102.
Shi T, Reeves RH, Gilichinsky DA, Friedmann EI. 1997. Characterization of viable bacteria from Siberian permafrost by 16S rDNA sequencing. *Microbial Ecology* 33: 169–179.
Shmakova L, Bondarenko N, Smirnov A. 2016. Viable species of Flamella (Amoebozoa: Variosea) isolated from ancient Arctic permafrost sediments. *Protist* 167: 13–30.
Shmakova LA, Karpov SA, Malavin SA, Smirnov AV. 2018. Morphology, biology and phylogeny of Phalansterium arcticum sp. n. (Amoebozoa, Variosea), isolated from ancient Arctic permafrost. *European Journal of Protistology* 63: 117–129.
Siddiqui R, Khan NA. 2012. Biology and pathogenesis of Acanthamoeba. *Parasites & Vectors* 5: 6–6.
Simmons M, Ochoterena H. 2000. Gaps as characters in sequence-based phylogenetic analyses. *Systematic Biology* 49: 369–381.
Stothard DR, Schroeder-Diedrich JM, Awwad MH, Gast RJ, Ledee DR, Rodriguez-Zaragoza S, Dean CL, Fuerst PA, Byers TJ. 1998. The evolutionary history of the genus Acanthamoeba and the identification of eight new 18S rRNA gene sequence types. *Journal of Eukaryotic Microbiology* 45: 45–54.
Stoupin D, Kiss AK, Arndt H, Shatilovich AV, Gilichinsky DA, Nitsche F. 2012. Cryptic diversity within the choanoflagellate morphospecies complex Codosiga botrytis – Phylogeny and morphology of ancient and modern isolates. *European Journal of Protistology* 48: 263–273.
Tice AK, Shadwick LL, Fiore-Donno AM, Geisen S, Kang S, Schuler GA, Spiegel

FW, Wilkinson KA, Bonkowski M, Dumack K, Lahr DJG, Voelcker E, Clauß S, Zhang J, Brown MW. 2016. Expansion of the molecular and morphological diversity of Acanthamoebidae (Centramoebida, Amoebozoa) and identification of a novel life cycle type within the group. *Biology Direct* 11.
Vishnivetskaya TA. 2009. Viable Cyanobacteria and Green Algae from the Permafrost Darkness. In: Margesin R, ed. *Permafrost Soils*. Berlin, Heidelberg: Springer Berlin Heidelberg, 73–84.
Visvesvara GS, Balamuth W. 1975. Comparative studies on related free-living and pathogenic amebae with special reference to Acanthamoeba. *The Journal of Protozoology* 22: 245–256.
Walochnik J, Obwaller A, Aspöck H. 2000. Correlations between morphological, molecular biological, and physiological characteristics in clinical and nonclinical isolates of Acanthamoeba spp. *Applied and Environmental Microbiology* 66: 4408–4413.
Yashina S, Gubin S, Maksimovich S, Yashina A, Gakhova E, Gilichinsky D. 2012. Regeneration of whole fertile plants from 30,000-y-old fruit tissue buried in Siberian permafrost. *Proceedings of the National Academy of Sciences of the United States of America* 109: 4008–4013.
Zanina OG, Gubin SV, Kuzmina SA, Maximovich SV, Lopatina DA. 2011. Late-Pleistocene (MIS 3-2) palaeoenvironments as recorded by sediments, palaeosols, and ground-squirrel nests at Duvanny Yar, Kolyma lowland, northeast Siberia. *Quaternary Science Reviews* 30: 2107–2123.